Analytical Eye-Diagram Determination for the Efficient and Accurate Signal Integrity Verification of Coupled Interconnect Lines

Minji Lee, Dongchul Kim, and Yungseon Eo

Abstract—**A new efficient analytical eye-diagram determination technique for coupled interconnect lines is presented. Two coupled lines are decoupled into isolated eigen modes; bit blocks for coupled lines, which are defined as a block of consecutive bits, are then represented with decoupled modes. The crosstalk effects within the bit blocks are taken into account. Thereby, the crucial input bit patterns for the worst case eye-diagram determination are modeled mathematically, including inter-symbol interference (ISI). The proposed technique shows excellent agreement with the SPICE-based simulation. Furthermore, it is very computation-time-efficient in the order of magnitude, compared with the SPICE simulation, which requires numerous pseudo-random bit sequence (PRBS) input signals.**

Index Terms—**Eye-diagram, jitter, transmission line, inter-symbol interference (ISI), signal integrity**

I. INTRODUCTION

In high-speed digital systems, signal integrity exacerbation due to interconnect lines significantly limits circuit performance [1-9]. Thus, the signal integrity verification of interconnect lines has become an integral part of the system design.

An eye-diagram is a helpful metric for intuitively and quickly assessing the performance quality of digital signals [10, 11]. The performance of interconnect lines can be easily estimated based on jitter and eye opening that can be readily determined from the eye-diagram. Since accurate eye-diagram determination requires a huge amount of computation time, many efficient eye-pattern determination techniques have been developed [12-27].

Among them, the peak distortion analysis (PDA) method [12] can determine the eye-diagram efficiently and accurately for symmetrically switching linear circuits. For asymmetrically switching linear circuits, the double edge rate (DER) method [14] can determine the eye-diagram accurately. However it is noteworthy that both PDA and DER method are not accurate enough to be employed for non-linear driver circuit model. In addition, unlike in isolated transmission lines, electromagnetic coupling between lines has a considerable effect on the signal integrity deterioration in coupled lines. In practice, each line has virtually random bit streams. Thus, the accurate eye-diagram determination of coupled lines requires much more computation time than that of single isolated lines since many PRBS signals have to be applied to both lines.

This paper presents an efficient signal integrity verification method for two coupled lines using analytical eye-diagram determination. For the sake of the analytical eye-diagram determination, coupled lines are first decoupled into eigen modes using the modal decoupling technique, thus allowing the coupled lines to be treated as isolated lines. However, for coupled lines, other effects due to crosstalk and switching within bit

Manuscript received Mar. 26, 2013; accepted Aug. 11, 2013
Department of Electronics and Communication Engineering, Hanyang University, Gyeonggi-do 425-791, Korea
E-mail : eo@giga.hanyang.ac.kr

blocks have to be taken into account. The overview of the coupled line analysis for eye-diagram determination is shown schematically in Fig. 1. The computation time of the proposed technique is comparable with the PDA technique [12].

In this study, we first determine essential basic modes by decoupling the two coupled lines. Necessary input test patterns for coupled line eye-diagram determination are then formulated mathematically. Next, further considerations for model accuracy improvement are discussed, and the accuracy and efficiency of the proposed technique are verified. Finally, the paper is summarized and concluded.

II. Coupled Line Analysis using Modal Decoupling

In a single isolated line, the simplest input signal model for the determination of ISIs can be formulated mathematically with only three constituents. Unlike the single isolated line, however, additional effects have to be taken into account for coupled lines. In practice, since coupling effects are too complicated to be treated directly, coupled signals are usually decoupled for analytical modeling of the signal transients. The two coupled lines shown in Fig. 2 have two eigen modes (even and odd mode for two identical lines). The signal transients of each line can be represented as a linear combination of each eigen mode, allowing them to be treated as a single isolated line [28].

An arbitrary n-bit stream (X) can be represented by a sequence of bits:

$$X = x_1 x_2 \cdots x_{i-1} x_i x_{i+1} \cdots x_{n-1} x_n \tag{1}$$

where $x_i \in \{0, 1\}$. Defining a part of this consecutive bit set as a bit block, the bit stream X can be represented with bit blocks as shown below

$$X = (x_1 x_2 x_3)(x_4 \cdots x_{i-1} x_i)(x_{i+1} \cdots x_{n-1} x_n) = B_1 B_2 B_3 \tag{2}$$

where the three bit blocks are $B_1 = x_1 x_2 x_3$, $B_2 = x_4 \cdots x_{i-1} x_i$, $B_3 = x_{i+1} \cdots x_{n-1} x_n$ respectively. For the bit blocks, the coupled lines can then be decoupled into

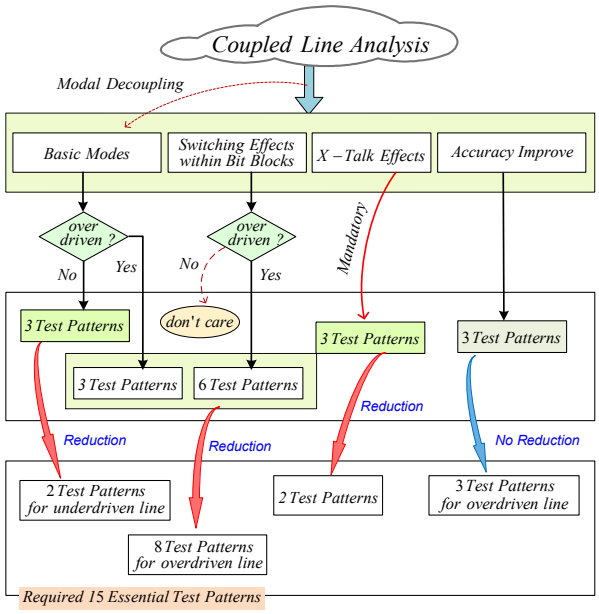

Fig. 1. Overview of coupled line analysis.

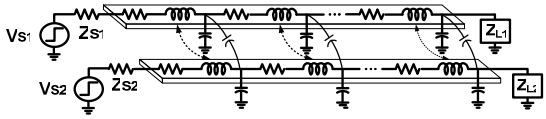

Fig. 2. Coupled lines.

three basic bit pattern combinations, as summarized in Table 1. Regarding a bit block as a lumped signal, like a single bit, the bit blocks have three types of switching patterns: i) a quiet state in which all the bits are in a quiet state, ii) a switching state in which at least one bit within a bit block is switching, and iii) the same switching pattern as ii) but with exactly reversed bit polarities that are common in differential signaling. Respective bit patterns for the bit blocks are represented with an arrow symbol; $(0, \uparrow, \downarrow)$=(quiet, positive switching pattern, negative switching pattern). Since all of the bit blocks can be represented with the three basic modes (i.e., $\uparrow\uparrow, \uparrow\downarrow, \uparrow 0$), the modal decoupling technique can be exploited. However, since coupling due to the presence of different switching bits between lines within a bit block cannot be adequately treated only with the modal decoupling technique, additional coupling mechanisms have to be considered.

Table 1. Combinations of bit blocks of two lines. Gray colored rows (3 rows) in X are basic modes, and Y is an additional mode. "$\langle\updownarrow\rangle$" indicates that the switching is arbitrary. The angle brackets "$\langle\cdot\rangle$" indicate a bit block

	bit blocks (<line1>,<line2>)	line of interest	Description of status	Fundamental modes?	effectively single ?
X	$(\langle 0\rangle, \langle 0\rangle)$	nothing	trivial	(no)	(yes)
	$(\langle 0\rangle, \langle\uparrow\rangle)$	line_1,2	line_1 victim	(yes)	(yes)
	$(\langle 0\rangle, \langle\downarrow\rangle)$	nothing	$(\langle 0\rangle, \langle\uparrow\rangle)$	(no)	(yes)
	$(\langle\uparrow\rangle, \langle 0\rangle)$	nothing	$(\langle 0\rangle, \langle\uparrow\rangle)$	(no)	(yes)
	$(\langle\uparrow\rangle, \langle\uparrow\rangle)$	line_1	even mode	(yes)	(yes)
	$(\langle\uparrow\rangle, \langle\downarrow\rangle)$	both lines	odd mode	(yes)	(yes)
	$(\langle\downarrow\rangle, \langle 0\rangle)$	nothing	$(\langle 0\rangle, \langle\downarrow\rangle)$	(no)	(yes)
	$(\langle\downarrow\rangle, \langle\uparrow\rangle)$	nothing	$(\langle\uparrow\rangle, \langle\downarrow\rangle)$	(no)	(yes)
	$(\langle\downarrow\rangle, \langle\downarrow\rangle)$	nothing	$(\langle\uparrow\rangle, \langle\uparrow\rangle)$	(no)	(yes)
Y	$(\langle\uparrow\rangle, \langle\updownarrow\rangle)$	coupling within a bit block		(yes)	Need waveform approx.

III. Input Test Patterns in a Single Line

In a single transmission line, if following two inequalities are satisfied,

$$Z_O > Z_S \quad \text{and} \quad \Gamma_L > \frac{Z_S Z_L - Z_O(Z_S + R_{DC})}{Z_O Z_L + Z_O(Z_S + R_{DC})} \tag{3}$$

a line is defined as an over-driven line since its output signal transient may have a multi-tonic wave-shape. Otherwise, the line is defined as an under-driven line [27]. The parameters Z_O, Z_S, Z_L, Γ_L, and R_{DC} are line characteristic impedance, source impedance, load impedance, reflection coefficient at the load, and dc resistance, respectively. Note that if a pulsed signal is transmitted through a transmission line, its original pulse shape is deformed due to various undesirable effects such as loss, dispersion, and reflection, etc. Typically, its pulse width is lengthened and its tail is dragged with sporadic

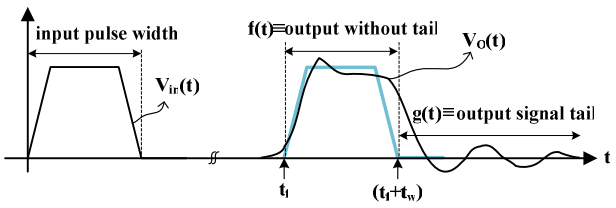

Fig. 3. Transmitted signal deformation.

ripple signals as shown in Fig. 3. Eye-diagrams can be readily determined with a few specific scenarios that may build-up eye-diagram boundaries. Thus, the simplest input signal model is characterized with three variables (i.e., t_A, t_B, and t_C, where t_A, t_B, and t_C are the previous signal pulse width, the time interval between the previous and present signal, and the present signal pulse width, respectively). For an input signal with a pulse width (t_W), the output signal can be mathematically formulated with two signal components (i.e., output signal without tail and output signal tail) as

$$v_o(t) = f(t) + g(t) \tag{4}$$

where

$$f(t) \equiv v_o(t)\left[u\left(t - t_f\right) - u\left(t - \left(t_f + t_w\right)\right)\right] \tag{5}$$

$$g(t) \equiv v_o(t) \cdot u\left(t - \left(t_f + t_w\right)\right) \tag{6}$$

where $g(t)$ can be considered a tail signal (see the right side of Fig. 3) and t_f is the time of flight. Regarding an input signal wave-shape as a simple square pulse, the previous signal can be formulated as

$$v_{in(A)}(t) = V_{DD}\left[u(t) - u\left(t - t_A\right)\right] \tag{7}$$

$$v_{o(A)}(t) = f_{o(A)}(t) + g_{o(A)}(t) \tag{8}$$

where

$$\begin{cases} f_{o(A)}(t) \equiv v_{o(A)}(t)\left[u\left(t - t_f\right) - u\left(t - \left(t_f + t_A\right)\right)\right] \\ g_{o(A)}(t) \equiv v_{o(A)}(t) \cdot u\left(t - \left(t_f + t_A\right)\right) \end{cases} \tag{9}$$

and the subscript "A" indicates the previous signal. Similarly, the present signal can be formulated as

$$v_{in(C)}(t) = V_{DD}\left[u\left(t-\left(t_A+t_B\right)\right)-u\left(t-\left(t_A+t_B+t_C\right)\right)\right] \tag{10}$$

$$v_{o(C)}(t) = f_{o(C)}\left(t\right)+g_{o(C)}\left(t\right) \tag{11}$$

where

$$\begin{cases} f_{o(C)}(t) \equiv v_{o(C)}\left(t\right)\left[u\left(t-\left(t_f+t_A+t_B\right)\right)\right. \\ \qquad\qquad \left.-u\left(t-\left(t_f+t_A+t_B+t_C\right)\right)\right] \\ g_{o(C)}(t) \equiv v_{o(C)}\left(t\right)\cdot u\left(t-\left(t_f+t_A+t_B+t_C\right)\right) \end{cases} \tag{12}$$

and the subscripts " B " and " C " indicate the time interval between signals and the present signal, respectively. Now that ISI between two neighboring signals can be paraphrased as the overlap between $g_{o(A)}\left(t\right)$ and $f_{o(C)}\left(t\right)$, the most crucial input signal modeling is to determine the three variables (i.e., t_A, t_B, and t_C). The parameter determination methods can be summarized in [27].

IV. INPUT TEST PATTERNS IN COUPLED LINES

Input signal may be deteriorated during the propagation due to energy loss, reflection, and coupling, etc. Thus, the propagated signal at the receiving end is dispersed with a long tail signal. Particularly, the long tail signal may continue to interact with subsequent signals (symbols). The interaction that is called ISI has a considerable effect on the eye-closing. In order to take the ISI effect into account, as in a single line, the test input signals for the coupled lines are formulated with six model parameters (i.e., $t_A^{line\_i}$, $t_B^{line\_i}$, and $t_C^{line\_i}$, where $t_A^{line\_i}$, $t_B^{line\_i}$, and $t_C^{line\_i}$ are the previous signal pulse width, the time interval between the previous and present signal, and the present signal pulse width of the *i*-th line, respectively). Such generic formulation, however, requires many test input signals. Comparing the magnitude of the previous tail signals and the present signals that has no tail signal depending on switching condition, the number of the necessary test input signals can be reduced. This will be discussed in the ensuing subsections.

1. Possible Switching Modes

Since the ISI analyses for the over-driven line are different from those of the under-driven line, whether a line is over-driven or under-driven needs to be distinguished. Moreover, signal transients in coupled lines are strongly correlated with the characteristic impedances, which depend upon the input switching patterns.

Assuming $Z_{S1}=Z_{S2}$ and $Z_{L1}=Z_{L2}$, either of the two categories can be readily discriminated as in a single isolated line. In the *i*-th line, if $\Gamma_{Li} < \left[Z_{Si}Z_{Li}-Z_{Oi}(Z_{Si}+R_{DCi})\right]/\left[Z_{Oi}Z_{Li}+Z_{Oi}(Z_{Si}+R_{DCi})\right]$, the line is an under-driven line. Otherwise, the line is an over-driven line. Once the lines are decoupled, they can be considered two isolated lines. According to Theorem 2 in [27], the worst case input signal model parameters for under-driven lines can then be determined as ($t_A=0$, $t_B=0$, and $t_C=t_{bit}$). Note that t_{bit} indicates a single bit duration. In contrast, according to Theorem 3 in [27], the worst case input signal model parameters for over-driven lines can be determined as ($t_A=2t_f$, $t_B=2t_f-t_C$, and $t_C=t_{bit}$). Since the previous signals in under-driven lines have no effect on the present signal, ISI can be determined using only the three possible input switching patterns described in Table 2. In contrast, since the previous signal tails in over-driven lines may have a significant effect on the present signal, there are nine possible input switching patterns, as summarized in Table 3. Therefore, if coupling effects are not considered, total 12 independent input test patterns are required.

The input signals can be formulated mathematically in a simple form using a unit step function. First, in the under-driven lines, the present signals can be represented using the unit step function.

$$\begin{aligned} v_{in(C)}^{line\_1}(t) = V_{DD}\Big[&u\left(t-(t_A^{line\_1}+t_B^{line\_1})\right) \\ &-u\left(t-(t_A^{line\_1}+t_B^{line\_1}+t_C^{line\_1})\right)\Big] \\ &\forall (t_A^{line\_1}=0, t_B^{line\_1}=0, t_C^{line\_1}=t_{bit}) \end{aligned} \tag{13}$$

$$\begin{aligned} v_{in(C)}^{line\_2}(t) = V_{DD}\Big[&u\left(t-(t_A^{line\_2}+t_B^{line\_2})\right) \\ &-u\left(t-(t_A^{line\_2}+t_B^{line\_2}+t_C^{line\_2})\right)\Big] \\ &\forall (t_A^{line\_2}=0, t_B^{line\_2}=0, t_C^{line\_2}=t_{bit}) \end{aligned} \tag{14}$$

In over-driven lines, the previous signals (positive pulse signals) can be represented as

$$v_{in(A)}^{line\_1}(t) = V_{DD}\left[u(t) - u\left(t - t_A^{line\_1}\right)\right],\ \forall t_A^{line\_1} = 2t_f \tag{15}$$

$$v_{in(A)}^{line\_2}(t) = V_{DD}\left[u(t) - u\left(t - t_A^{line\_2}\right)\right],\ \forall t_A^{line\_2} = 2t_f \tag{16}$$

Assuming that the time duration of line_1 between the previous signal and present signal is $t_B^{line\_1}$, the present signal can be represented as

$$\begin{aligned} v_{in(C)}^{line\_1}(t) = V_{DD}\Big[&u\left(t - (t_A^{line\_1} + t_B^{line\_1})\right) \\ &-u\left(t - (t_A^{line\_1} + t_B^{line\_1} + t_C^{line\_1})\right)\Big] \\ &\forall (t_B^{line\_1} = 2t_f - t_C^{line\_1}, t_C^{line\_1} = t_{bit}) \end{aligned} \tag{17}$$

Similarly, the present signal in line_2 can be represented as

$$\begin{aligned} v_{in(C)}^{line\_2}(t) = V_{DD}\Big[&u\left(t - (t_A^{line\_2} + t_B^{line\_2})\right) \\ &-u\left(t - (t_A^{line\_2} + t_B^{line\_2} + t_C^{line\_2})\right)\Big] \\ &\forall (t_B^{line\_2} = 2t_f - t_C^{line\_2}, t_C^{line\_2} = t_{bit}) \end{aligned} \tag{18}$$

2. Reduction of Input Test Patterns

In coupled lines, without considering coupling effects, the minimum number of input test patterns for ISI determination is 12, as summarized in Tables 2 and 3. In reality, if signal transient modulations due to crosstalk and switching are taken into account, six additional input test patterns are required. Therefore, total 18 input test patterns are typically necessary for the eye-diagram determination of coupled lines. However, if the line characteristics and signal transient variations are scrutinized, the number of necessary input test patterns is reduced from 18 to 15. The input test pattern reduction theory can be summarized as in Theorems 1 and 2.

Theorem 1: In two coupled over-driven lines, if the previous signal duration of line_1 is "$t_A^{line\_1} = 2t_f$" and $R_{DC} \approx 0$, the magnitude of the tail signal is reduced to its minimum value. The magnitudes for the three possible switching patterns are ordered as

$$\begin{aligned} &\min\left[[g_{o(A)}^{line\_1}(t)]^{\uparrow\uparrow}\right] < \min\left[[g_{o(A)}^{line\_1}(t)]^{\uparrow 0}\right] \\ &< \min\left[[g_{o(A)}^{line\_1}(t)]^{\uparrow\downarrow}\right],\ \forall\ Z_S Z_L > Z_O^{\uparrow\uparrow} Z_O^{\uparrow 0} \end{aligned} \tag{19}$$

Table 2. Input signals for under-driven lines

Switching time		Case	Input
Previous	Present		
No previous signal	↑↑	U1	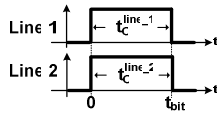
	↑0	U2	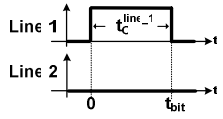
	↑↓	U3	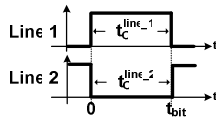

$$\begin{aligned} &\min\left[[g_{o(A)}^{line\_1}(t)]^{\uparrow\uparrow}\right] > \min\left[[g_{o(A)}^{line\_1}(t)]^{\uparrow 0}\right] \\ &> \min\left[[g_{o(A)}^{line\_1}(t)]^{\uparrow\downarrow}\right],\ \forall\ Z_S Z_L < Z_O^{\uparrow 0} Z_O^{\uparrow\downarrow} \end{aligned} \tag{20}$$

Proof: Without coupling, according to Theorem 3 in [27], when the previous signal duration in line_1 (which is assumed to be a lossless line) is $t_A^{line\_1} = 2t_f$, the resulting value is $\min[g_{o(A)}^{line\_1}(t)]$ in the time interval of $(3t_f < t < 5t_f)$, which is

$$g_{o(A)}^{line\_1}(t) = V_{int}(1 + \Gamma_L)\Gamma_L\Gamma_G = PQ,\ \forall (3t_f < t < 5t_f) \tag{21}$$

where $P \equiv V_{int}(1 + \Gamma_L)$ and $Q \equiv \Gamma_L\Gamma_G$.

Since "$Z_O^{\uparrow\uparrow} > Z_O^{\uparrow 0} > Z_O^{\uparrow\downarrow}$", the respective magnitudes of P depending on switching condition have the relationship as below

$$P^{\uparrow\uparrow} > P^{\uparrow 0}, \quad \forall\ Z_S Z_L > Z_O^{\uparrow\uparrow} Z_O^{\uparrow 0} \tag{22}$$

$$P^{\uparrow 0} > P^{\uparrow\downarrow}, \quad \forall\ Z_S Z_L > Z_O^{\uparrow 0} Z_O^{\uparrow\downarrow} \tag{23}$$

$$P^{\uparrow\uparrow} < P^{\uparrow 0}, \quad \forall\ Z_S Z_L < Z_O^{\uparrow\uparrow} Z_O^{\uparrow 0} \tag{24}$$

$$P^{\uparrow 0} < P^{\uparrow\downarrow}, \quad \forall\ Z_S Z_L < Z_O^{\uparrow 0} Z_O^{\uparrow\downarrow} \tag{25}$$

Further, since "$Z_O^{\uparrow\uparrow} Z_O^{\uparrow 0} > Z_O^{\uparrow 0} Z_O^{\uparrow\downarrow}$" (22)-(25) can be rearranged by

$$P^{\uparrow\uparrow} > P^{\uparrow 0} > P^{\uparrow\downarrow}, \quad \forall\ Z_S Z_L > Z_O^{\uparrow\uparrow} Z_O^{\uparrow 0} \tag{26}$$

$$P^{\uparrow\uparrow} < P^{\uparrow 0} < P^{\uparrow\downarrow}, \quad \forall\ Z_S Z_L < Z_O^{\uparrow 0} Z_O^{\uparrow\downarrow} \tag{27}$$

Table 3. Input signals for over-driven lines

Switching time		Case	Input
Previous	Present		
↑↑	↑↑	O1	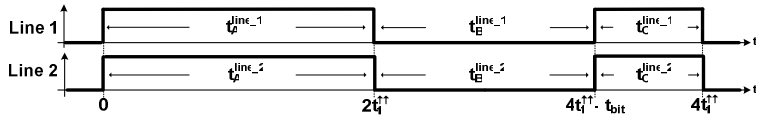
	↑0	O2	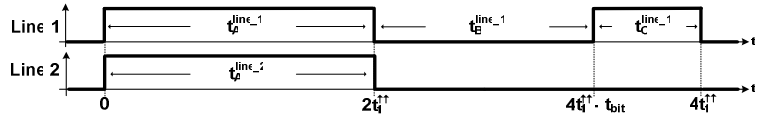
	↑↓	O3	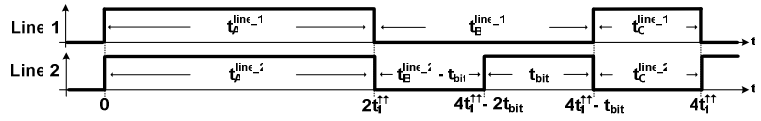
↑0	↑↑	O4	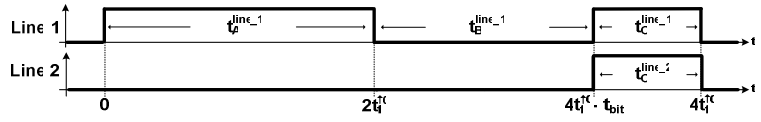
	↑0	O5	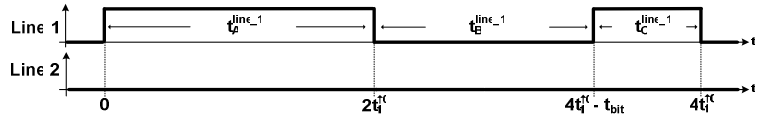
	↑↓	O6	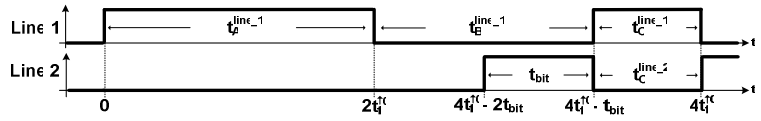
↑↓	↑↑	O7	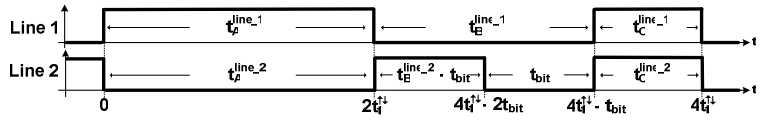
	↑0	O8	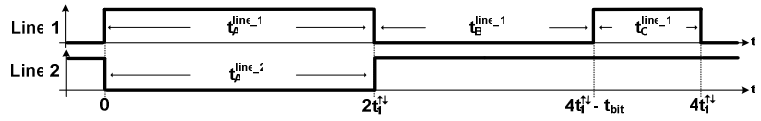
	↑↓	O9	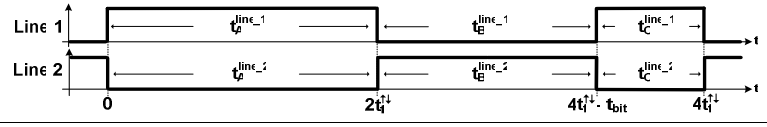

In an over-driven line, according to Theorem 3 in [27], $Q<0$. In this case, the magnitudes of Q with switching conditions are

$$\left|Q^{\uparrow\uparrow}\right|>\left|Q^{\uparrow 0}\right|, \quad \forall\ Z_S Z_L > Z_O^{\uparrow\uparrow} Z_O^{\uparrow 0} \tag{28}$$

$$\left|Q^{\uparrow 0}\right|>\left|Q^{\uparrow\downarrow}\right|, \quad \forall\ Z_S Z_L > Z_O^{\uparrow 0} Z_O^{\uparrow\downarrow} \tag{29}$$

$$\left|Q^{\uparrow\uparrow}\right|<\left|Q^{\uparrow 0}\right|, \quad \forall\ Z_S Z_L < Z_O^{\uparrow\uparrow} Z_O^{\uparrow 0} \tag{30}$$

$$\left|Q^{\uparrow 0}\right|<\left|Q^{\uparrow\downarrow}\right|, \quad \forall\ Z_S Z_L < Z_O^{\uparrow 0} Z_O^{\uparrow\downarrow} \tag{31}$$

As before, since "$Z_O^{\uparrow\uparrow} Z_O^{\uparrow 0} > Z_O^{\uparrow 0} Z_O^{\uparrow\downarrow}$", (28)-(31) can be rearranged by

$$\left|Q^{\uparrow\uparrow}\right|>\left|Q^{\uparrow 0}\right|>\left|Q^{\uparrow\downarrow}\right|, \quad \forall\ Z_S Z_L > Z_O^{\uparrow\uparrow} Z_O^{\uparrow 0} \tag{32}$$

$$\left|Q^{\uparrow\uparrow}\right|<\left|Q^{\uparrow 0}\right|<\left|Q^{\uparrow\downarrow}\right|, \quad \forall\ Z_S Z_L < Z_O^{\uparrow 0} Z_O^{\uparrow\downarrow} \tag{33}$$

Thus,

$$\left|\left[PQ\right]^{\uparrow\uparrow}\right| > \left|\left[PQ\right]^{\uparrow 0}\right| > \left|\left[PQ\right]^{\uparrow\downarrow}\right|, \quad \forall\ Z_S Z_L > Z_O^{\uparrow\uparrow} Z_O^{\uparrow 0} \tag{34}$$

$$\left|\left[PQ\right]^{\uparrow\uparrow}\right| < \left|\left[PQ\right]^{\uparrow 0}\right| < \left|\left[PQ\right]^{\uparrow\downarrow}\right|, \quad \forall\ Z_S Z_L < Z_O^{\uparrow 0} Z_O^{\uparrow\downarrow} \tag{35}$$

Therefore (19) and (20) are valid. ■

Theorem 2: In two coupled lines, if the present signal duration of line_1 is "$t_C^{line\_1} = t_{bit}$" at a given bit rate, the magnitude of the present signal becomes the minimum peak value. The magnitudes of the three possible switching patterns are ordered as

$$\begin{aligned}\max\left[\left[f_{o(C)}^{line\_1}(t)\right]^{\uparrow\uparrow}\right] &> \max\left[\left[f_{o(C)}^{line\_1}(t)\right]^{\uparrow 0}\right] \\ &> \max\left[\left[f_{o(C)}^{line\_1}(t)\right]^{\uparrow\downarrow}\right], \quad \forall\ Z_S Z_L > Z_O^{\uparrow\uparrow} Z_O^{\uparrow 0}\end{aligned} \tag{36}$$

$$\begin{aligned}\max\left[\left[f_{o(C)}^{line\_1}(t)\right]^{\uparrow\uparrow}\right] &< \max\left[\left[f_{o(C)}^{line\_1}(t)\right]^{\uparrow 0}\right] \\ &< \max\left[\left[f_{o(C)}^{line\_1}(t)\right]^{\uparrow\downarrow}\right], \quad \forall\ Z_S Z_L < Z_O^{\uparrow 0} Z_O^{\uparrow\downarrow}\end{aligned} \tag{37}$$

Proof: Assuming a signal that switches toward a logical high state from a logical low state, since the signal requires a finite transient time, a short pulse duration may not reach a steady state value. Thus, the worst case bit duration occurs for a single bit at a given bit rate. Without coupling, when the present signal duration in line_1 (which is assumed to be a lossless line) is $t_C^{line\_1} = t_{bit}$, the resulting value is the minimum peak value:

$$\max[f_{o(C)}^{line\_1}(t)] = V_{int}(1+\Gamma_L) = P \tag{38}$$

According to Theorem 1, the magnitude of this value under switching conditions is

$$P^{\uparrow\uparrow} > P^{\uparrow 0} > P^{\uparrow\downarrow}, \qquad \forall\ Z_S Z_L > Z_O^{\uparrow\uparrow} Z_O^{\uparrow 0} \tag{39}$$

$$P^{\uparrow\uparrow} < P^{\uparrow 0} < P^{\uparrow\downarrow}, \qquad \forall\ Z_S Z_L < Z_O^{\uparrow 0} Z_O^{\uparrow\downarrow} \tag{40}$$

Therefore (36) and (37) are valid. ■

In under-driven lines, the minimum eye-heights become

$$V_{U1}^{upper} = \max\left[\left[f_{o(C)}^{line\_1}(t)\right]^{\uparrow\uparrow}\right], \ \forall\ Z_S Z_L < Z_O^{\uparrow 0} Z_O^{\uparrow\downarrow} \tag{41}$$

$$V_{U3}^{upper} = \max\left[\left[f_{o(C)}^{line\_1}(t)\right]^{\uparrow\downarrow}\right], \ \forall\ Z_S Z_L > Z_O^{\uparrow\uparrow} Z_O^{\uparrow 0} \tag{42}$$

where the superscript "upper" implies the upper bound of the eye-height and the subscript Ui indicates the case-i of the under-driven lines (see Table 2).

In over-driven lines, the eye-height is strongly correlated with the previous input signal switching patterns. When the previous input switching patterns are "$\uparrow\uparrow$", the eye-height boundaries are

$$\begin{aligned}V_{O1}^{upper} &= \min\left[\left[g_{o(A)}^{line\_1}(t)\right]^{\uparrow\uparrow}\right] + \max\left[\left[f_{o(C)}^{line\_1}(t)\right]^{\uparrow\uparrow}\right] \\ &\quad \forall\ Z_S Z_L < Z_O^{\uparrow 0} Z_O^{\uparrow\downarrow}\end{aligned} \tag{43}$$

$$\begin{aligned}V_{O2}^{upper} &= V_{O3}^{upper} \\ &= \min\left[\left[g_{o(A)}^{line\_1}(t)\right]^{\uparrow\uparrow}\right] + \max\left[\left[f_{o(C)}^{line\_1}(t)\right]^{\uparrow 0}\right] \\ &\quad \forall\ Z_S Z_L > Z_O^{\uparrow\uparrow} Z_O^{\uparrow 0}\end{aligned} \tag{44}$$

where the subscript Oi indicates the case-i of the over-driven lines (see Table 3). In contrast, when the previous input switching pattern is in the "$\uparrow 0$" switching mode, the eye-height boundaries are

$$\begin{aligned}V_{O4}^{upper} &= \min\left[\left[g_{o(A)}^{line\_1}(t)\right]^{\uparrow 0}\right] + \max\left[\left[f_{o(C)}^{line\_1}(t)\right]^{\uparrow\uparrow}\right] \\ &\quad \forall\ Z_S Z_L < Z_O^{\uparrow 0} Z_O^{\uparrow\downarrow}\end{aligned} \tag{45}$$

$$\begin{aligned}V_{O6}^{upper} &= \min\left[\left[g_{o(A)}^{line\_1}(t)\right]^{\uparrow 0}\right] + \max\left[\left[f_{o(C)}^{line\_1}(t)\right]^{\uparrow\downarrow}\right] \\ &\quad \forall\ Z_S Z_L > Z_O^{\uparrow\uparrow} Z_O^{\uparrow 0}\end{aligned} \tag{46}$$

Similarly, when the previous input switching pattern is in the "$\uparrow\downarrow$" switching mode, the eye-height boundaries are

$$\begin{aligned}V_{O7}^{upper} &= V_{O8}^{upper} \\ &= \min\left[\left[g_{o(A)}^{line\_1}(t)\right]^{\uparrow\downarrow}\right] + \max\left[\left[f_{o(C)}^{line\_1}(t)\right]^{\uparrow 0}\right] \\ &\quad \forall\ Z_S Z_L < Z_O^{\uparrow 0} Z_O^{\uparrow\downarrow}\end{aligned} \tag{47}$$

$$\begin{aligned}V_{O9}^{upper} &= \min\left[\left[g_{o(A)}^{line\_1}(t)\right]^{\uparrow\downarrow}\right] + \max\left[\left[f_{o(C)}^{line\_1}(t)\right]^{\uparrow\downarrow}\right] \\ &\quad \forall\ Z_S Z_L > Z_O^{\uparrow\uparrow} Z_O^{\uparrow 0}\end{aligned} \tag{48}$$

Note that, according to Theorem 1,

$$\min\left[\left[g_{o(A)}^{line\_1}(t)\right]^{\uparrow\uparrow}\right] > \min\left[\left[g_{o(A)}^{line\_1}(t)\right]^{\uparrow 0}\right] \quad \forall\ Z_S Z_L < Z_O^{\uparrow 0} Z_O^{\uparrow\downarrow} \tag{49}$$

$$\min\left[\left[g_{o(A)}^{line\_1}(t)\right]^{\uparrow\downarrow}\right] > \min\left[\left[g_{o(A)}^{line\_1}(t)\right]^{\uparrow 0}\right] \quad \forall\ Z_S Z_L > Z_O^{\uparrow\uparrow} Z_O^{\uparrow 0} \tag{50}$$

Thus, since

$$V_{O1}^{upper} > V_{O4}^{upper},\ \forall\ Z_S Z_L < Z_O^{\uparrow 0} Z_O^{\uparrow\downarrow} \tag{51}$$

$$V_{O9}^{upper} > V_{O6}^{upper},\ \forall\ Z_S Z_L > Z_O^{\uparrow\uparrow} Z_O^{\uparrow 0} \tag{52}$$

the O1 and O9 input patterns can be neglected.

In summary, the eye-height upper bound for under-driven lines can be determined using only the response wave-shapes of the U1 and U3 input patterns. In contrast, it is unknown whether any of the six input test patterns is the worst case for over-driven lines. Thus, the eye-height upper bound for the over-driven lines can be determined using the response wave-shapes of the six input test patterns (i.e., V_{O2}^{upper}, V_{O3}^{upper}, V_{O4}^{upper}, V_{O6}^{upper}, V_{O7}^{upper}, and V_{O8}^{upper}). Therefore, if the coupling effects are put aside, 8 input test patterns are sufficient to determine the eye-diagram of the coupled lines. However, as mentioned previously, additional effects that modulate the transient signal have to be taken into account.

3. Wave-Shape Distortion due to Coupling

In coupled lines, electromagnetic coupling between the lines (i.e., crosstalk) considerably distorts the signal transient wave-shapes. Note that the eye-height upper bound may be formed when the crosstalk signal due to the previous input switching is added to the present input signal. Thus, the coupling effects also have to be taken into account for accurate eye-diagram determination. As shown in Fig. 4, regardless of the line characteristics (under-driven or over-driven), if a negative input step pulse is applied to line_2, the absolute magnitude of the far-end crosstalk (FEXT) signal becomes a maximum in the time interval $t_f < t < 3t_f$ [29]. Since the crosstalk signal is generally a monotonically decreasing wave-shape in the time interval, it is assumed that $\min[v_o^{line\_1}(t)]$ occurs at $3t_f^-$. The eye-height upper bound occurs when the present input signal is aggravated by the maximum crosstalk signal due to the previous input switching patterns. Furthermore, since the present signal always has the minimum value when its bit duration is 1 bit at a given bit rate, the input signal model parameters of line_1 for the eye-height upper bound due to the crosstalk are $t_A^{line\_1} = 0$, $t_B^{line\_1} = 2t_f^{\uparrow 0} - t_{bit}$, and $t_C^{line\_1} = t_{bit}$.

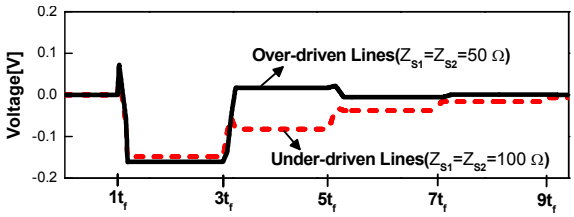

Fig. 4. Far-end coupling due to negative step input (FEXT). Lossless line, $Z_{L1} = Z_{L2} = \infty$, and line length=5 cm.

There are three possible present input signal switching

Table 4. Additional input signal due to crosstalk

Switching Time		Case	Input
Previous	Present		
Negative step input of line_2	↑↑	A1	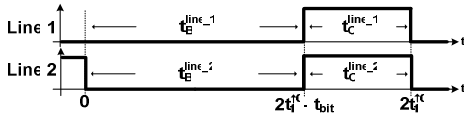
	↑0	A2	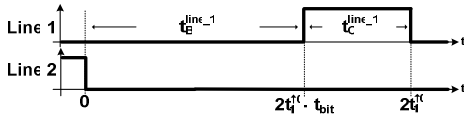
	↑↓	A3	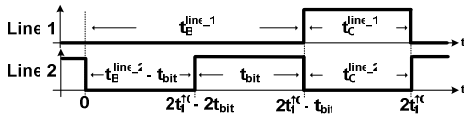

patterns. The input signals for respective switching patterns are summarized in Table 4. Note that either the case A2 or the case A3 may produce the eye-height boundary. The wave-shape can be formulated as

$$\begin{aligned} V_{A2}^{upper} &= V_{A3}^{upper} \\ &= \min[v_o^{line\_1}(t)] + \max\left[[f_{o(C)}^{line\_1}(t)]^{\uparrow 0}\right] \end{aligned} \tag{53}$$

In summary, two additional input test patterns are necessary in order to account for the crosstalk effects.

V. Accuracy Improvement in the Model

1. Accuracy Improvement for Eye-Height and Jitter

In the over-driven lines, the eye-height upper bound and jitter are modulated due to crosstalk. An example is shown in Fig. 5(a). Thus, for more accurate eye-diagram determination, this modulation effect has to be taken into account. The eye-diagram considering the signal transient modulation effect can be determined with the following input switching patterns:

$$\begin{cases} v_{in}^{line\_1}(t) = V_{DD}\left[u(t) - u(t - 4t_f^{\uparrow\uparrow})\right] \\ v_{in}^{line\_2}(t) = V_{DD}\left[u(t) - u(t - 2t_f^{\uparrow\uparrow})\right] \end{cases} \tag{54}$$

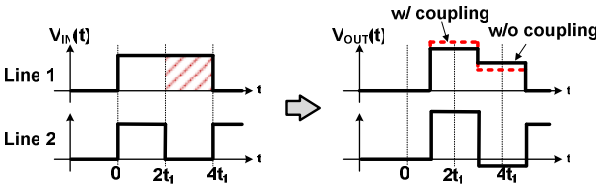

(a)

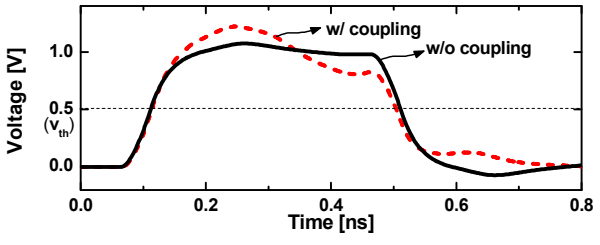

(b)

Fig. 5. Additional bit stream for over-driven lines. The worst eye-height occurs near oblique lines. $Z_{S1} = Z_{S2} = 50\Omega$, $C_{L1} = C_{L2} = 0.5\,pF$, and line length=1 cm (a) Coupling effects due to line_2, (b) Signal transient.

$$\begin{cases} v_{in}^{line\_1}(t) = V_{DD}\left[u(t) - u(t - 4t_f^{\uparrow\uparrow})\right] \\ v_{in}^{line\_2}(t) = V_{DD}\left[u(t) - u(t - 2t_f^{\uparrow\uparrow}) + u(t - 4t_f^{\uparrow\uparrow})\right] \end{cases} \tag{55}$$

Furthermore, as shown in Fig. 6(a), if $Z_S Z_L > Z_O^{\uparrow\uparrow} Z_O^{\uparrow 0}$, the edge rate of the even mode switching is greater than that of the odd mode switching. The fastest rising edge signal that arrives at v_{th} is either the even mode switching or the odd mode switching, whereas the fastest falling edge signal that arrives at v_{th} is the odd mode switching signal. In over-driven lines, if $Z_S Z_L > Z_O^{\uparrow\uparrow} Z_O^{\uparrow 0}$, the output signal magnitude for a bit input signal is greater in even mode switching than in odd mode switching. In this case, according to Theorem 1, the maximum tail signal occurs with even mode switching. Thus, for more accurate jitter estimation, additional input test signals in which the previous signal is in even mode and the present signal is in even or odd mode have to be taken into account. A switching pattern in which the previous and present signals are in even mode switching is described in the case O1 of Table 3. Switching in which the previous signal is in even mode and the present signal is in odd mode is described in the case O3 of Table 3.

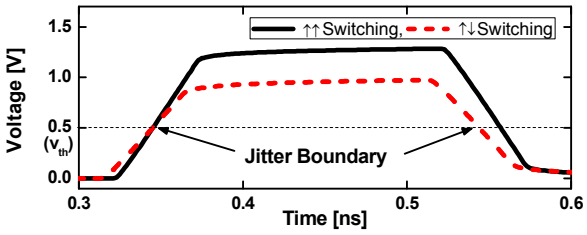

(a)

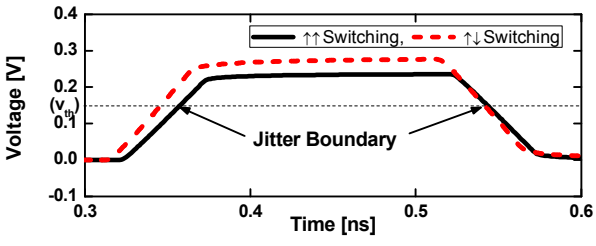

(b)

Fig. 6. Switching-mode-dependent output signal magnitudes for a bit input signal. $Z_{S1} = Z_{S2} = 50\Omega$ and line length=5 cm (a) $Z_S Z_L > Z_O^{\uparrow\uparrow} Z_O^{\uparrow 0}$ and $Z_{L1} = Z_{L2} = \infty$, (b) $Z_S Z_L < Z_O^{\uparrow 0} Z_O^{\uparrow\downarrow}$ and $Z_{L1} = Z_{L2} = 20\Omega$.

Thus, either of the two lines has a spurious bit signal between the previous signal and present signal. If this is not the case, the odd mode present signal cannot be generated. In other words, there exists an additional 10 (or 01) switching pattern between the previous even mode switching and the present odd mode switching. Thus, in this switching case, before the present signal switches to the odd mode, signal coupling due to the additional 10 (or 01) switching pattern between the previous and present switching patterns has an effect on the present signal switching. Moreover, as shown in Fig. 6(a), the falling edge jitter is affected by the odd mode switching that arrives at v_{th} earlier. In this case, the falling edge jitter can be determined more accurately using the following input signals:

$$\begin{cases} v_{in}^{line\_1}(t) = V_{DD}\left[u(t)-u(t-2t_f^{\uparrow\uparrow})+u(t-4t_f^{\uparrow\uparrow}-t_{bit}) \right. \\ \qquad\qquad \left. -u(t-4t_f^{\uparrow\uparrow})\right] \\ v_{in}^{line\_2}(t) = V_{DD}\left[u(t)-u(t-2t_f^{\uparrow\uparrow})+u(t-4t_f^{\uparrow\uparrow})\right] \end{cases} \tag{56}$$

In the over-driven line, if $Z_S Z_L < Z_O^{\uparrow 0} Z_O^{\uparrow\downarrow}$, the output signal magnitude for a bit input signal is larger in odd mode switching than in even mode switching, as shown in Fig. 6(b). In this case, according to Theorem 1, the maximum tail signal occurs with odd mode switching. Thus, for more accurate jitter estimation, additional input test signals in which the previous signal is odd mode and the present signal is even or odd mode have to be taken into account. The case O7 describes a switching pattern in which the previous signal is in odd mode and the present signal is in even mode. The case O9 describes a switching pattern in which both the present and previous signals are in odd mode. These two cases also have to be taken into account.

In summary, not only the new switching patterns defined in (54), (55), and (56) but also the cases O1 and O9 have to be taken into account for more accurate jitter determination.

2. Bit Conversion

Now that the input test patterns are formulated in terms of flight time (analog information), they need to be adjusted to be a practical input signals. Input switching patterns for eye-diagram determination are formulated using the time of flight (i.e., t_f). Since t_f is a function of the input switching pattern, the values for each pattern are represented as follows:

$$\begin{aligned} t_f^{\uparrow\uparrow} &= \sqrt{(L_{11}+L_{12})C_{11}} \\ &\approx \sqrt{(L_{11}+L_{12})(C_{11}+C_L)} \end{aligned} \tag{57}$$

$$\begin{aligned} t_f^{\uparrow\downarrow} &= \sqrt{(L_{11}-L_{12})(C_{11}+2C_{12})} \\ &\approx \sqrt{(L_{11}-L_{12})(C_{11}+2C_{12}+C_L)} \end{aligned} \tag{58}$$

$$\begin{aligned} t_f^{\uparrow 0} &\approx \sqrt{L_{11}(C_{11}+C_{12})} \\ &\approx \sqrt{L_{11}(C_{11}+C_{12}+C_L)} \end{aligned} \tag{59}$$

where L_{11}, L_{12}, C_{11}, C_{12}, and C_L are self inductance, mutual inductance, self capacitance, mutual capacitance, and load capacitance, respectively. Now that t_f has to be represented in terms of the number of bit, it is converted according to the following rule: $I[t_x^{line\_i}]^j \geq 1,\ \forall i, j \in \{1,2\}$.

The $t_x^{line\_i}$ indicates the one of the 3 time duration of the *i*-th line (i.e., $t_A^{line\_i}$, $t_B^{line\_i}$, and $t_C^{line\_i}$). The superscript indicates "upper bound (*j*=1) or lower bound (*j*=2)".

3. General Input Signal Model with Multiple Interferences

Up to now, only one previous signal has been considered in the simplest input signal model for ISI. However, for more general input signal model for ISI, multiple bit patterns have to be taken into account. In order to simplify the problem, since it is the same technique as that used for the single isolated line [27], we consider a scenario in which two previous signals have an effect on the present signal. The input signal with two previous signals can be schematically described as shown in Fig. 7. Nomenclatures for the input signal model parameters are defined as follows.

t_A : Time duration for previous signal#1

t_B : Time interval between two previous signals

t_C : Time duration for previous signal#2

t_D : Time interval between previous signal#2 and

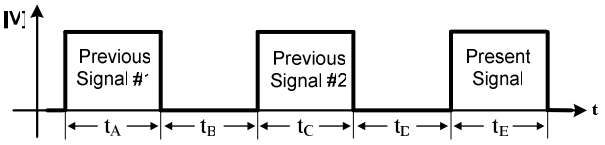

Fig. 7. Input signal model with two previous signals for a single line.

present signal

t_E : Time duration for present signal.

Note, Theorem 3 in [27] can be applied to the interaction between the present bit and the previous signal#2. Thus, the model parameters except for t_A and t_B can be determined as

$$\left(t_C = 2t_f, t_D = 2t_f - t_E, t_E = t_{bit}\right) \tag{60}$$

Since the maximum tail signal occurs after $2t_f$, $t_A = 2t_f$. Thus the input signal for the first previous signal and its output signal are

$$v_{in(A)}(t) = V_{DD}\left[u(t) - u(t - t_A)\right],\ \forall t_A = 2t_f \tag{61}$$

$$v_{o(A)}(t) = h(t) * v_{in(A)}(t) \tag{62}$$

In order for $v_{o(A)}(t)$ to be $\min[v_{o(A)}(t)]$, t_B has to be determined. With only one previous signal, the minimum value of the tail signal of the previous signal#1 exists in the time interval of $3t_f < t < 5t_f$. However, in the input signal with two previous signals, since the previous signal#2 (which has the bit duration $t_C = 2t_f$) follows the previous signal#1 after t_B, the present signal exists in the time interval $7t_f < t < 9t_f$. Thus, t_B has to be $2t_f$ (i.e., $t_B = 2t_f$). In summary, the model parameters for the input signal model with two previous signals are ($t_A = 2t_f$, $t_B = 2t_f$, $t_C = 2t_f$, $t_D = 2t_f - t_E$, and $t_E = t_{bit}$).

Note, the input signal model with the two previous signals can be readily generalized with minor modification for the n-input signal model of coupled lines. In this work, we employed 2-previous signal model which is considered accurate enough in most cases.

VI. VERIFICATION OF THE PROPOSED TECHNIQUE

In order to verify the efficiency and accuracy of the proposed technique, a test transmission line circuit as shown in Fig. 2 is evaluated using both PRBS-based SPICE simulation and the proposed technique [30, 31]. The circuit model parameters are $Z_{S1} = Z_{S2} = 100\Omega$ for under driven lines and $Z_{S1} = Z_{S2} = 50\Omega$ for over driven lines. The SPICE W-element model parameters of the transmission line are

$$R_{DC} = \begin{bmatrix} 0.23148 & 0.015964 \\ 0.015964 & 0.23148 \end{bmatrix} \frac{\Omega}{cm}$$

$$R_S = \begin{bmatrix} 36.564 & 5.4927 \\ 5.4927 & 36.564 \end{bmatrix} \frac{\mu\Omega}{cm\sqrt{Hz}}$$

$$L = \begin{bmatrix} 3.7595 & 1.227 \\ 1.227 & 3.7595 \end{bmatrix} \frac{nH}{cm}$$

$$C = \begin{bmatrix} 1.1941 & -0.36109 \\ -0.36109 & 1.1941 \end{bmatrix} \frac{pF}{cm}$$

Two distinct PRBS input signals are generated with a 16-stage linear feedback shift register (LFSR) composed of [16, 13, 9, 6] and [16, 10, 7, 4] feedback taps.

The eye-height and jitter for under-driven (see Fig. 8) and over-driven lines (see Fig. 9) using the proposed technique are compared with those of the PRBS-based SPICE simulation. As shown in Fig. 8, the eye-height and jitter for the under-driven lines have good agreement with each other since the SPICE simulation using the PRBS-based input signals includes the eye-boundaries in which the proposed technique generates. However, the jitter for the over-driven lines using SPICE simulation shows a discrepancy with that using the proposed technique because PRBS-based input signals still do not cover all of the possible input patterns of the proposed method, although large numbers of PRBS signals are employed.

The simulation results for the linear coupled lines of Fig. 2 are summarized in Table 5. The circuit model parameters are $Z_{S1} = Z_{S2} = 50\,\Omega$, $C_{L1} = C_{L2} = 0.5\,pF$, $t_{rise} = t_{fall} = 50\,ps$, and the bit rate of input signals is 5 Gb/s. The length of the transmission line is assumed as 5 cm long line and W-element model is employed for the

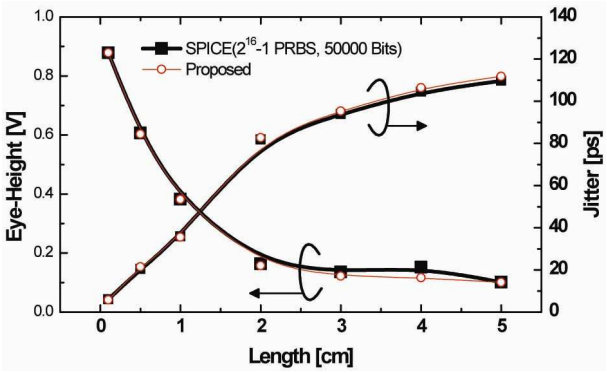

Fig. 8. Eye-height and jitter in coupled under-driven lines with variable line lengths. $Z_{S1} = Z_{S2} = 100\Omega$, $C_{L1} = C_{L2} = 0.5\,pF$, $t_{rise} = t_{fall} = 50\,ps$, and bit rate=5 Gb/s.

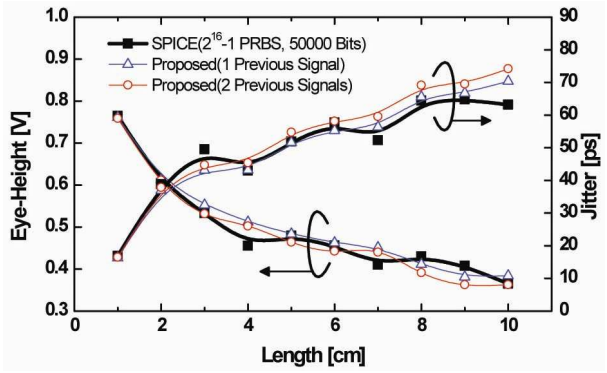

Fig. 9. Eye-height and jitter in coupled over-driven lines with variable line lengths. $Z_{S1} = Z_{S2} = 50\Omega$, $C_{L1} = C_{L2} = 0.5\,pF$, $t_{rise} = t_{fall} = 50\,ps$, and bit rate=5 Gb/s.

Table 5. Eye-height and jitter of linear circuits

	SPICE			Proposed	Casper [12]
	1×10^4 Bits	3×10^4 Bits	5×10^4 Bits		
Height [mV]	499.3	482.7	479.6	464.0	459.5
Jitter [ps]	50.7	51.9	51.9	55.5	56.1
Time [s]	146	863	2110	3	2.23

circuit simulation. As shown in Table 5, if the number of the random vectors increases, SPICE simulation shows much better agreement with the proposed technique. As shown in Table 5, the proposed technique shows the similar accuracy as the PDA in the linear circuits. However, in the non-linear circuit (see Fig. 10), as shown in Table 6, the eye-height using PDA is too pessimistic while the jitter is too optimistic. In contrast, both the eye-height and jitter using the proposed technique show good agreement with SPICE simulation using PRBS input signals. Note that the circuit model parameters except for

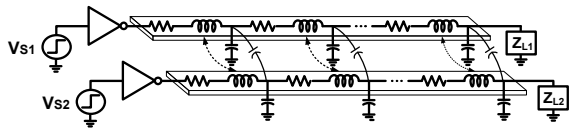

Fig. 10. Non-linear coupled lines.

Table 6. Eye-height and jitter of non-linear circuits

	SPICE			Proposed	Casper [12]
	1×10^4 Bits	3×10^4 Bits	5×10^4 Bits		
Height [mV]	379.6	357.2	356.0	335.0	224.7
Jitter [ps]	78.2	78.4	79.0	79.9	105.8
Time [s]	298	1306	2865	134	2.23

the input drivers are the same as in the linear circuit.

The proposed technique was implemented with MATLAB 9.0 in a PC that uses a 2.4 GHz Intel Core2 Quad CPU Q6600 with 4 GByte DDR2 RAM. In order to achieve reasonable accuracy using the PRBS-based SPICE simulation, 5×10^4 PRBSs were applied to both lines. Note that, in general, since the PRBS-based SPICE simulation requires excessive computation time even in a single line, it is considered impractical for coupled lines. However, the biggest problem of the PRBS-based SPICE simulation for coupled lines is that the worst case bit stream cannot be guaranteed even if the number of PRBSs is increased. Therefore, the proposed technique is considered useful for practical applications.

VII. CONCLUSIONS

In high-speed integrated circuits and systems, the inter-symbol interference noise due to interconnect lines between the circuit sub-blocks is one of the significant circuit failure mechanisms. This paper presents a new efficient and accurate eye pattern determination technique for coupled lines and verifies its accuracy. To achieve this, a few fundamental bit stream patterns that may induce the worst case ISI are mathematically formulated. Since this method determines the eye-diagram using only a few bit patterns, it is highly efficient with respect to computation time compared with the PRBS-based SPICE simulation, which inefficiently employs numerous PRBS input signals. The technique can be used for signal integrity verification or design of high-speed integrated systems.

ACKNOWLEDGMENTS

This research was supported by the Basic Science Research Program through the National Research Foundation of Korea (NRF) funded by the Ministry of Education, Science and Technology (Grant number 2011-0025655).

REFERENCES

[1] International technology roadmap for semiconductors, 2009. [Online]. Available: http://www.itrs.net.

[2] R. Nair, "Effect of increasing chip density on the evolution of computer architectures," *IBM J. Res. & Dev*., vol. 46, no. 2/3, pp. 223-234, Mar./May 2002.

[3] R. Berridge et al., "IBM POWER6 microprocessor physical design and design methodology," *IBM J. Res. & Dev*., vol. 51, no. 6, pp. 685-714, Nov. 2007.

[4] N. Kurd, P. Mosalikanti, M. Neidengard, J. Douglas, and R. Kumar, "Next generation Intel® core™ micro-architecture (Nehalem) clocking," *IEEE J. Solid-State Circuits*, vol. 44, no. 4, pp. 1121-1129, Apr. 2009.

[5] M. Bohr, "The new era of scaling in an SoC world," in *Proc. ISSCC*, 2009, pp. 23-28.

[6] Y. Kudoh, M. Fukaishi, and M. Mizuno, "A 0.13-μm CMOS 5-Gb/s 10-m 28AWG cable transceiver with no-feedback-loop continuous-time post-equalizer," *IEEE J. Solid-State Circuits*, vol. 38, no. 5, pp. 741-746, May 2003.

[7] D. N. de Araujo, J. Diepenbrock, M. Cases, and N. Pham, "Transmitter and channel equalization for high-speed server interconnects," in *Proc. EPEP*, 2003, pp. 221-224.

[8] J. D. Meindl, "Beyond Moore's law: the interconnect era," *IEEE Comput. Sci. Eng. Mag*., vol. 5, no. 1, pp. 20-24, Jan./Fab. 2003.

[9] P. Pulici et al., "Signal integrity flow for system-in-package and package-on-package devices," *Proc. IEEE*, vol. 97, no. 1, pp. 84-95, Jan. 2009.

[10] N. Ou, T. Farahmand, A. Kuo, S. Tabatabaei, and A. Ivanov, "Jitter models for the design and test of Gbps-speed serial interconnects," *IEEE Des. Test. Comput*., vol. 21, no. 4, pp. 302-313, Jul.-Aug. 2004.

[11] G. Breed, "Analyzing signals using the eye diagram," *High Frequency Electronics*, pp. 50-52, Nov. 2005.

[12] B. Casper, M. Haycock, and R. Mooney, "An accurate and efficient analysis method for multi-Gb/s chip-to-chip signaling schemes," in *Symp. VLSI Circuits Dig. Tech. Papers*, 2002, pp. 54-57.

[13] B. Casper et al., "Future microprocessor interfaces: analysis, design and optimization," in *Proc. CICC*, 2007, pp. 479-486.

[14] R. Shi, W. Yu, Y. Zhu, C. Cheng, and E. S. Kuh, "Efficient and accurate eye diagram prediction for high speed signaling," in *Proc. ICCAD*, 2008, pp. 655-661.

[15] W. Yu, R. Shi, and C. Cheng, "Accurate eye diagram prediction based on step response and its application to low-power equalizer design," *IEICE Trans. Electron*, vol. E92-C, no. 4, pp. 444-452, Apr. 2009.

[16] W. Yao, Y. Shi, L. He, S. Pamarti, and Y. Hu, "Worst case timing jitter and amplitude noise in differential signaling," in *Proc. ISQED*, 2009, pp. 40-46.

[17] J. Ren and K. S. Oh, "Multiple edge responses for fast and accurate system simulations," *IEEE Trans. Adv. Packag*., vol. 31, no. 4, pp. 741-748, Nov. 2008.

[18] A. Tsuchiya, Y. Gotoh, M. Hashimoto, and H. Onodera, "Performance limitation of on-chip global interconnects for high-speed signaling," in *Proc. CICC*, 2004, pp. 489-492.

[19] A. Tsuchiya, M. Hashimoto, and H. Onodera, "Optimal termination of on-chip transmission-lines for high-speed signaling," *IEICE Trans. Electron*, vol. E90-C, no. 6, pp. 1267-1273, Jun. 2007.

[20] M. Hashimoto, J. Siriporn, A. Tsuchiya, H. Zhu, and C. Cheng, "Analytical eye-diagram model on-chip distortionless transmission lines and its application to design space exploration," *IEICE Trans. Fundamentals*, vol. E91-A, no. 12, pp. 3474-3480, Dec. 2008.

[21] W. Guo, J. Lin, C. Lin, T. Huang, and R. Wu, "Fast methodology for determining eye diagram characteristics of lossy transmission lines," *IEEE Trans. Adv. Packag*., vol. 32, no. 1, pp. 175-183, Feb. 2009.

[22] K. S. Oh et al., "Accurate system voltage and timing margin simulation in high-speed I/O system

designs," *IEEE Trans. Adv. Packag*., vol. 31, no. 4, pp. 722-730, Nov. 2008.

[23] D. Oh, J. Ren, and S. Chang, "Hybrid statistical link simulation technique," *IEEE Trans. Compon. Packag. Manuf. Technol*., vol. 1, no. 5, pp. 772-783, May 2011.

[24] J. Buckwalter, B. Analui, and A. Hajimiri, "Predicting data-dependent jitter," *IEEE Trans. Circuits Syst. II, Exp. Briefs*, vol. 51, no. 9, pp. 453-457, Sep. 2004.

[25] B. Analui, J. F. Buckwalter, and A. Hajimiri, "Data-dependent jitter in serial communications," *IEEE Trans. Microw. Theory Tech*., vol. 53, no. 11, pp. 3388-3397, Nov. 2005.

[26] H. Zhu, C. Cheng, A. Deutsch, and G. Katopis, "Predicting and optimizing jitter and eye-opening based on bitonic step response," in *Proc. EPEP*, 2007, pp. 155-158.

[27] D. Kim, H. Kim, and Y. Eo , "Analytical eye-diagram determination for the efficient and accurate signal integrity verification of singal integrity verification of single interconnect lines," *IEEE Trans. Comput.-Aided Des. Integr. Syst*., vol. 31, no. 10, pp. 1536-1545, Oct. 2012.

[28] T. Kim and Y. Eo, "Analytical CAD models for signal transients and crosstalk noise of inductance-effect-prominent multi-coupled RLC interconnect lines," *IEEE Trans. Comput.-Aided Des. Integr. Syst*., vol. 27, no. 7, pp.1214-1227, Jul. 2008.

[29] J. A. DeFalco, "Reflection and crosstalk in logic circuit interconnections," *IEEE Spectrum*, pp. 44-50, Jul. 1970.

[30] *HSPICE Signal Integrity User Guide Version A-2008.03*, Synopsys, Inc., Mountain View, CA.

[31] MathWorks, *MATLAB*, [Online]. Available: http://www.mathworks.com

Minji Lee received the B.S. in electrical and computer engineering from Hanyang University, Ansan, Korea, in 2011, and the M.S. degree in the department of information display engineering, Hanyang University, Korea, in 2013. Her research interests are high-frequency characterization, modeling, and simulation concerned with the signal integrity verification of high-speed integrated systems.

Dongchul Kim received the B.S. and M.S. degrees in electrical and computer engineering from Hanyang University, Ansan, Korea, in 2007 and 2009, respectively. He is currently working toward the Ph.D. degree in electrical and computer engineering from Hanyang University. His research interests are high-frequency characterization, modeling, and simulation concerned with the signal integrity verification of high-speed integrated circuits, and high-speed data link design.

Yungseon Eo received the B.S. and M.S. in electronic engineering from Hanyang University, Seoul, Korea, in 1983 and 1985, respectively, and the Ph.D. in electrical engineering from the University of Florida, Gainesville, FL, in 1993. From 1986 to 1988, he was with the Korea Telecommunication Authority Research Center, Seoul, Korea, where he performed telecommunication network planning and software design. From 1993 to 1994, he worked for Applied Micro Circuits Corporation, San Diego, CA, where he performed S-parameter-based device characterization and modeling for high-speed CMOS circuit design. From 1994 to 1995, he was at the Research and Development Center of LSI Logic Corporation, Santa Clara, CA, where he worked in the signal integrity characterization and modeling of high-speed CMOS circuits and interconnects. From 2004 to 2005, he was with High-Speed Microelectronics Group as a guest researcher at the National Institute of Standards and Technology (NIST), Boulder, CO. From 2011 to 2012, he was with Infrastructure Design Center as a consulting professor, Samsung Electronics, Gyeonggi-do, Korea. He is now a professor of electronics and communication engineering at Hanyang University, Ansan, Korea. His research interests are high-frequency characterization, modeling, and simulation concerned with integrated circuits interconnects, integrated circuit packaging, and system level integration technology.